

1 **Characterizing Leaf Area Index (LAI) and Vertical Foliage** 2 **Profile (VFP) over the United States**

3

4 **H. Tang¹, S. Ganguly², G. Zhang², M. A. Hofton¹, R. F. Nelson³, and R. Dubayah¹**

5 [1] {Department of Geographical Sciences, University of Maryland, College Park, Maryland,
6 USA}

7 [2] {Bay Area Environmental Research Institute (BAERI) / NASA Ames Research Center,
8 Moffett Field, California, USA}

9 [3] {Biospheric Sciences Branch, Code 618, NASA Goddard Space Flight Center, Greenbelt,
10 Maryland, USA}

11 Correspondence to: H. Tang (htang@umd.edu)

12

13 **Abstract**

14 Leaf area index (LAI) and vertical foliage profile (VFP) are among the important canopy
15 structural variables. Recent advances in lidar remote sensing technology have demonstrated the
16 capability of accurately mapping LAI and VFP over large areas. The primary objective of this
17 study was to derive and validate a LAI and VFP product over the contiguous United States
18 (CONUS) using spaceborne waveform lidar data. This product was derived at the footprint level
19 from the Geoscience Laser Altimeter System (GLAS) using a biophysical model. We validated
20 GLAS derived LAI and VFP across major forest biomes using airborne waveform lidar. The
21 comparison results showed that GLAS retrievals of total LAI were generally accurate with little
22 bias ($r^2 = 0.67$, bias = -0.13, RMSE = 0.75). The derivations of GLAS retrievals of VFP within
23 layers was not as accurate overall ($r^2 = 0.36$, bias = -0.04, RMSE = 0.26), and these varied as a
24 function of height, increasing from understory to overstory - 0 to 5 m layer: $r^2 = 0.04$, bias =
25 0.09, RMSE = 0.31; 10 to 15 m layer: $r^2 = 0.53$, bias = -0.08, RMSE = 0.22; and 15 to 20 m layer:
26 $r^2 = 0.66$, bias = -0.05, RMSE = 0.20. Significant relationships were also found between GLAS

1 LAI products and different environmental factors, in particular elevation and annual precipitation.
2 In summary, our results provide a unique insight into vertical canopy structure distribution across
3 North American ecosystems. This data set is a first step towards a baseline of canopy structure
4 needed for evaluating climate and land use induced forest changes at continental scale in the
5 future and should help deepen our understanding of the role of vertical canopy structure on
6 terrestrial ecosystem processes across varying scales.

7

8 **1 Introduction**

9 Accurate measurements of three dimensional canopy structure and function play a key role in
10 global carbon dynamics, climate feedbacks as well as biodiversity studies (Heimann and
11 Reichstein, 2008;Loreau et al., 2001;Cramer et al., 2001;Schimel et al., 2001). Spatial variations
12 of ecosystem structure largely inform the geographical patterns of ecological processes, including
13 species richness (Cramer et al., 2001;Goetz et al., 2007;Turner et al., 2003). These structural
14 variables, such as canopy height, leaf area index (LAI) and vertical foliage profile (VFP), have
15 been identified as essential climate variables (ECV), essential biodiversity variables (EBV) or
16 both (Pereira et al., 2013;Aber, 1979;Gower and Norman, 1991;Baret et al., 2013). Yet
17 measurements of these canopy structural data are often limited at field sites, and their spatial
18 distributions over broader geographical areas still remain poorly characterized due to
19 heterogeneity of natural vegetation and inexact measuring techniques (Clark and Kellner,
20 2012;Asner et al., 2013). Improved spatial characterization of LAI and VFP at large scales may
21 fill this observational gap and help clarify the role of spatial and vertical variability in canopy
22 structure for carbon cycling, biodiversity and habitat quality (Houghton, 2007;Sauer et al., 2008).

23 Several global scale LAI products have been created from passive remote sensing data for many
24 years (Myneni et al., 2002;Ganguly et al., 2012;Deng et al., 2006;Baret et al., 2007). Most of
25 these products are derived by exploring the correlation between canopy foliage density and the
26 total reflected intensity of electromagnetic radiation at multiple wavelengths. Applications of
27 these LAI products have significantly improved the representation of the dynamics of terrestrial
28 ecosystems and their interactions with the atmosphere (Mu et al., 2007;Zhao et al.,
29 2005;Randerson et al., 2009). However, the overall accuracy of these products does not meet the

1 requirements as specified by Global Terrestrial Observing System (GTOS:
2 <http://www.fao.org/gtos/org.html>), and a key problem is the saturation of spectral signal over
3 dense forests with high canopy cover (Abuelgasim et al., 2006;Shabanov et al., 2005;Yang et al.,
4 2006). Saturation occurs because the solar flux decreases exponentially as it passes through a
5 dense canopy, and the majority of the returned signal comes from the upper canopy in the form of
6 direct reflectance and multiple scattering (Gower and Norman, 1991;Nilson, 1971). This limits
7 the observational capabilities of passive optical sensors, such as Landsat and MODIS, to estimate
8 LAI over dense forests. Furthermore, deriving the foliage profile as a function of height is beyond
9 the capability of passive optical remote sensing unless multiple look angles are used (Chopping et
10 al., 2009). We argue that spaceborne lidar (light detection and ranging) technology provides a
11 means of overcoming this limitation and of measuring vertical structure even over dense forests.

12 Lidar has proven effective at measuring three dimensional canopy structural information (Lefsky
13 et al., 2002). Lidar measures the distance between a target and the sensor by the round-trip
14 traveling time of an emitted laser pulse. It allows direct 3D measurements of canopy structural
15 components, including foliage, branch and trunk which then be used to estimate biophysical
16 variables, such as canopy height and biomass (Drake et al., 2002;Saatchi et al., 2011;Los et al.,
17 2012;Lefsky, 2010;Simard et al., 2011;Asner et al., 2012;Baccini et al., 2012;Strahler et al.,
18 2008), as well as LAI and VFP (Morsdorf et al., 2006;Tang et al., 2012;Zhao et al., 2013).

19 Garcia et al. (2012) and Luo et al. (2013) demonstrated the possibility of deriving LAI and VFP
20 data across different landscapes from Geoscience Laser Altimeter System (GLAS) on board of
21 Ice, Cloud and land Elevation Satellite (ICESat). Tang et al. (2014a) derived LAI and VFP data
22 from GLAS data, but using a physically based model rather than an empirical methodology. The
23 use of a physical model greatly simplified application over large areas because site specific,
24 statistical calibrations were not required. Further improvement of the model led to a GLAS LAI
25 and VFP product over the entire state of California, USA (Tang et al., 2014b). However, there is
26 still a need to further examine the relationship between vertical foliage distribution and lidar
27 waveforms over even broader areas. Assessment of their relationship across different forest types
28 and environmental gradients will not only strengthen our confidence in acquiring a potential
29 global LAI and VFP measurement, but will also provide guidance on the design and science

1 definition of future lidar missions such as the Global Ecosystem Dynamics Investigation (GEDI)
2 (Dubayah et al., 2014).

3 The objective of this study is to characterize the continental scale variability of canopy structure
4 across the United States using lidar observations from space. First, we implement our existing
5 algorithm at the GLAS footprint level and compare the derived data with LAI and VFP products
6 from airborne lidar in different forest types. Next we map the aggregated LAI and VFP product
7 according to different ecoregions and land cover types over the Contiguous United States
8 (CONUS). Finally we analyze the distribution of GLAS LAI across different environmental
9 factors, including elevation and precipitation.

10

11 **2 Methods**

12 **2.1 GLAS Data**

13 GLAS is a spaceborne, sampling waveform lidar sensor with the working wavelength in the near-
14 infrared band (1064 nm). It emits laser pulses at a frequency of 40 Hz and records the energy
15 reflected from both the ground surface and canopy in an approximately 65 m diameter footprint
16 (Abshire et al., 2005). GLAS samples the Earth surface in transects with individual footprints
17 separated by ~ 175 m along track, and with between track spacing that varies as a function of
18 latitude (e.g. 30 km spacing between tracks at the equator and 5 km spacing at 80° latitude
19 (Brenner et al., 2012)). As a result of this sampling pattern, GLAS does not provide a wall-to-
20 wall observation of forests. Its spatial allocation of laser footprints is best defined as a pseudo-
21 systematic sampling or cluster sampling strategy (Stahl et al., 2011;Healey et al., 2012). To
22 obtain a spatially continuous estimate of LAI at continental scale, footprint level GLAS data
23 would need to be extrapolated using other remote sensing data (Dubayah et al., 2008;Lefsky,
24 2010), or can be mapped into appropriate geographic strata such as land cover types or
25 ecoregions.

1 **2.2 Retrieval of GLAS LAI and VFP**

2 We collected a total of 1,100,498 cloud-free GLAS data from Campaigns GLA01 and GLA14
3 data over the contiguous United States from 2003 to 2007. GLA01 included the complete
4 recorded waveform at a vertical resolution of 15 cm for land surface products, and GLA14
5 products were comprised of geographical information and various parameters calculated from the
6 waveform (Harding and Carabajal, 2005). Low energy shots (peak energy < 0.5 Volt) were
7 excluded from data process for retrieval quality control because those waveforms were
8 susceptible to noise contamination. Shots during leaf-off season (November to March) were also
9 filtered out over deciduous forests and mixed forests. LAI and its profiles (0.15 m at vertical
10 resolution) were initially calculated for GLAS footprints based on a Geometric Optical and
11 Radiative Transfer (GORT) model (Ni-Meister et al., 2001), and further corrected for slope
12 effects using an iterative method (Tang et al., 2014a). Canopy VFP were calculated from
13 integration of footprint level LAI profiles at height intervals of 0 to 5 m, 5 to 10 m, 10 to 15 m
14 and 15 to 20 m. More details of the GLAS data processing can be found in the supplement.

15 **2.3 Comparison Data Sets**

16 We validated LAI and VFP data sets using an airborne lidar system, LVIS (Laser Vegetation
17 Imaging Sensor). LVIS is a medium resolution (~ 25 m diameter) waveform scanning lidar
18 system designed by NASA Goddard Space Flight Center (GSFC) (Blair et al., 1999). It can image
19 the terrestrial surface across a 2 km wide swath and has been deployed to map many different
20 forest structural parameters at regional scales across diverse biomes (Tang et al., 2012; Drake et
21 al., 2002; Swatantran et al., 2012). We calculated both total LAI and VFP at 5 m height intervals
22 from existing LVIS data using our physically based model, which has been validated using
23 different types of field measurements (destructive sampling, LAI-2000 and hemispherical photos)
24 (Tang et al., 2012; Tang et al., 2014a; Zhao et al., 2013). LVIS data used in this study included
25 major forest types from eastern, central and western US, including Maine forests just north of
26 Orono, Maine (2003), Sierra National Forest in California (2008), mixed forests along
27 Baltimore/Washington corridor (2003) and the White River National Wildlife Refuge in Arkansas
28 (2006). These LVIS datasets were all collected during leaf-on season.

1 We also included a 30 m resolution Landsat LAI map to examine the spatial distribution of
2 GLAS total LAI. Landsat has the longest earth observation history at moderate resolution (30 m),
3 and for decades has provided a consistent and unique measurement of terrestrial ecosystems. The
4 Landsat LAI map was produced using Global Land Survey (GLS) 2005 orthorectified Landsat
5 data (Ganguly et al., 2012; Ganguly et al., In Prep.).

6 **2.4 Analysis**

7 The comparison between LVIS and GLAS was performed at the GLAS footprint level. LVIS
8 shots falling within a 32.5 m radius from a GLAS shot center were selected. We filtered GLAS
9 footprints to have a minimum of 3 coincident LVIS shots to increase the likelihood that the LVIS
10 data covered a sufficient portion of the larger GLAS footprints. Both LAI and the 5 m interval
11 VFP of LVIS shots were averaged onto each coincident GLAS footprint for comparison. We also
12 made a footprint level comparison between GLAS LAI and the Landsat LAI map. A 3×3
13 Landsat window was applied to each GLAS footprint center to extract the averaged Landsat LAI
14 pixels. Pixels with invalid values (e.g. retrieval failure or non-vegetation pixel) were excluded in
15 the comparison. Agreements of different LAI datasets were assessed by coefficient of
16 determination, bias and RMSE (Root Mean Square Error):

$$17 \text{ bias} = \sum_{i=1}^n \frac{GLAS_i - Ref_i}{n} \quad (1)$$

$$18 \text{ RMSE} = \sqrt{\frac{\sum_{i=1}^n (GLAS_i - Ref_i)^2}{n}} \quad (2)$$

19 In Eq. (1) and Eq. (2), $GLAS_i$ is GLAS LAI (or VFP) value at footprint level and Ref_i is that
20 extracted from LVIS or Landsat.

21 Next, we aggregated the footprint level GLAS data into terrestrial ecoregions based on subset of a
22 global map (Olson et al., 2001). Statistical analysis of total LAI and LAI strata (VFP aggregated
23 at every 10 m height interval) was performed subsequently for each ecoregion. We also analyzed
24 the GLAS LAI and VFP distribution across different environmental gradients throughout
25 CONUS. GLAS footprints were categorized according to different environmental factors,
26 including vegetation type, topographic data and annual measurements of climate variables. The
27 vegetation map was derived from the MODIS Land Cover Type product (MCD12Q1) at 500 m

1 resolution following the IGBP scheme (Friedl et al., 2010). Elevation data was extracted from the
2 void-filled 90 m resolution SRTM (Shuttle Radar Topography Mission) DEM data (Reuter et al.,
3 2007). Precipitation, temperature and vapor pressure deficit information originated from the 800
4 m resolution 30yr annual normal climate data developed by the PRISM Climate Group (PRISM,
5 2013).

6 **3 Results**

7 This section includes three major parts: the first part focuses on the validation and comparison of
8 GLAS LAI and VFP data with existing products; the second presents the geographical
9 distribution of GLAS LAI and VFP, and; the last part shows their relationship with
10 environmental factors.

11 **3.1 GLAS LAI and VFP Comparisons with LVIS and Landsat**

12 The footprint level comparison between GLAS LAI and LVIS LAI had an overall r^2 of 0.60, bias
13 of -0.23, and RMSE of 0.82 (Fig. 1). Except for a few outliers at the lower range of LAI, most of
14 the comparison points were distributed along the 1:1 line suggesting no systematic difference
15 between the two data sets. No significant bias was found across individual sites either.

16 The agreement of the 5 m height interval VFP distributions between the two data sets was lower
17 than that of total LAI ($r^2 = 0.36$, a bias = -0.04 and RMSE = 0.26). Although there was no
18 systematic bias observed when all sites and vertical intervals are considered (Fig. 2), examination
19 by layer showed that GLAS overestimated understory LAI (0 to 5 m) ($r^2 = 0.04$, bias =
20 0.09, RMSE = 0.31) when compared with LVIS LAI (Fig. 3) but agreement improved as the
21 vertical height interval considered moved higher in the canopy (5 to 10 m, $r^2 = 0.33$, bias = -
22 0.13, RMSE = 0.29; and 10 to 15 m, $r^2 = 0.53$, bias = -0.08, RMSE = 0.22), reaching a maximum
23 at the top of the canopy (15 to 20 m, $r^2 = 0.66$, bias = -0.05, RMSE = 0.20).

24 The comparison between Landsat LAI and GLAS LAI had a much lower agreement than that of
25 LVIS ($r^2 = 0.18$, bias = 0.18 and RMSE = 2.02) (Fig. 4). Even though the two data sets agreed
26 well at lower LAI values, Landsat overestimated LAI at the middle range (from LAI values of 1
27 to 3) and then saturated above a value of about 4 to 5 against GLAS data.

1 **3.2 Aggregated GLAS LAI and VFP within Ecoregions**

2 We next mapped GLAS LAI across US ecoregions (Fig. 5). Highest LAI values were found along
3 northern Pacific Coast while lowest values occurred in the basin and range province and the arid
4 rains shadow region east of the Rocky Mountains. Northern California coastal forests (Pacific
5 temperate rainforests) were found to have the highest mean LAI value of 5.24. In the eastern
6 U.S., the mixed deciduous forests of the Appalachian-Blue Ridge province had the highest value
7 of 3.95 while other ecoregions around north-south direction of Appalachian Mountains had
8 similar LAI values around 3 ~ 4 (Table 1). Forest ecoregions with lowest LAI values (excluding
9 desert, shrubland and grassland) were located in Arizona mountains forests (1.15) and Great
10 Basin montane forests (0.90). Differences between these ecoregion-level LAI were significant
11 based on a bonferroni adjusted t-test, except for those among Willamette Valley forests,
12 Appalachian-Blue Ridge forests, Puget lowland forests and Appalachian mixed mesophytic
13 forests (p -values > 0.05).

14 LAI strata formed by VFP at each 10 m height interval were also averaged and mapped across the
15 US (Fig. 6). We chose the 10 m height interval rather than that of 5 m because LAI strata
16 aggregated at 10 m height interval represented a more accurate and reliable description of vertical
17 canopy structure given the relatively lower measurement accuracy in the understory (< 5 m) we
18 found in comparison to LVIS data. Each strata showed a generally similar geographic pattern as
19 that of total LAI with the decreasing trend from coast to interior lands, but the specific patterns
20 among strata differed. Northwestern forests were observed to have the highest total LAI values as
21 well as LAI strata values. Northern California coastal forests exhibited the largest total LAI value
22 as well as highest foliage density under 20 m height, while British Columbia mainland coastal
23 forests showed the highest foliage density (1.13) above 20 m height with a lower total LAI value
24 (4.74).

25 The distribution of GLAS total LAI and profiles were examined across different land cover types
26 (Fig. 7 and Fig. 8). Not surprisingly, forests were found to have a consistently greater value than
27 non-forest biomes in both total LAI and its strata. For example, deciduous broadleaf forests had
28 the highest value of total LAI (mean = 4.03) as well as that of middle and upper LAI strata
29 (height > 10 m), while open shrubland showed the lowest total LAI values of 0.77. However,
30 vertical LAI distributions of most forests and non-forests were similar with peak foliage density

1 distributed around a height of 2 ~ 4 m. The only exception was deciduous broadleaf forest, of
2 which most of leaves were distributed at middle-story level with a peak height at about 8 m. Its
3 VFP values did not decrease significantly until reaching a height of 15 m.

4 **3.3 GLAS LAI Distributions by Environmental Factors**

5 A linear regression analysis between GLAS LAI and SRTM DEM showed that increasing altitude
6 led to an overall decreasing, but non-monotonic, trend in LAI values ($LAI = 3.60 - 0.686 \times$
7 $Elevation (km)$, $r^2 = 0.59$, all $P < 0.01$) (Fig. 9). GLAS LAI values increased with DEM at the
8 elevation range from 0 to 750 m and 2000 to 3000 m. The variation in the LAI-DEM relationship
9 agreed well with Forest Ratio ($LAI = 0.112 + 3.18 \times Forest Ratio$, $r^2 = 0.45$, $P < 0.01$). Here each
10 GLAS footprint was classified as either forest or non-forest with an overlay of MODIS land cover
11 map, and the Forest Ratio was defined as the percentage of footprints classified as forests in total
12 GLAS shots within each elevation group. A multiple linear regression analysis showed that about
13 87% of total variance could be explained by a simple combination of elevation groups and Forest
14 Ratio values: $LAI = 2.59 \times Forest Ratio - 0.595 \times Elevation (km) + 1.58$.

15 We also analyzed GLAS LAI by 30yr normal annual climate data using linear regression models
16 (Fig. 10). It was observed that increasing precipitation significantly increased LAI values (ΔLAI
17 $= 1.84$ per 1000 mm precipitation increase) but only at low and moderate precipitation levels ($<$
18 2400 mm): $LAI = 1.84 \times precipitation (mm) \times 10^{-3} + 0.774$, $r^2 = 0.96$, $adj-r^2 = 0.95$, $P < 0.01$. It
19 contributed little when exceeding that threshold ($LAI = 0.22 \times precipitation (mm) \times 10^{-3}$, $r^2 =$
20 0.40 , $adj-r^2 = 0.30$, $P = 0.09$), as we found no significant LAI increase among groups greater
21 than 2400 mm using a bonferroni adjusted t-test. GLAS LAI was also negatively but slightly
22 correlated with minimum (maximum) vapor pressure deficit with a Pearson's correlation
23 coefficient of -0.29 (-0.15). The correlation coefficients between GLAS LAI and annual mean /
24 minimum / maximum temperature were even lower with values of 0.13, 0.18 and 0.08
25 respectively.

26 Finally, we applied multiple linear regression analysis to illustrate the combined environmental
27 effects of altitude and precipitation the on distributions of LAI and VFP. The regression analyses
28 were conducted at both GLAS footprint level and aggregated scale on altitude and precipitation
29 groups. At footprint level, altitude and precipitation together explained about 30% of variance of

1 total LAI ($LAI = 2.73 - 0.69 \times \text{Elevation (km)} + 0.58 \times \text{precipitation (mm)} \times 10^{-3}$, $r^2 = 0.29$, *adj-*
2 $r^2 = 0.29$, $P < 0.01$). However, their correlations with footprint level VFP (0 - 10 m, 10 - 20 m
3 and > 20 m height intervals) were not significant with r^2 of 0.07, 0.12 and 0.08 respectively. At
4 the aggregated scale, there was a better relationship between averaged LAI (VFP) values and
5 environmental factors. The combination of altitude and precipitation can explain more than 60%
6 variance in both total LAI and VFP, but explains only about 36% of variance on LAI for canopies
7 less than 10 m height.

8 **4 Discussion**

9 In this study, we generated GLAS estimates of LAI and VFP across the United States, validated
10 with an airborne lidar sensor, LVIS. Comparisons between LVIS and GLAS LAI and VFP
11 estimates in different forest types across the United States show that GLAS generally provides
12 accurate LAI and VFP estimates at footprint level. Considering the temporal offset and spatial
13 resolution differences between LVIS and GLAS, their overall agreements on LAI and VFP are
14 acceptable ($r^2 = 0.60$, bias = -0.23, and RMSE = 0.82; and $r^2 = 0.36$, bias = -0.043, and RMSE =
15 0.26). Our comparisons further demonstrate the efficacy of our retrieval methods over continental
16 scales that encompass large gradients in environmental factors and variability in forest types.

17 Measurement accuracy of GLAS VFP was lower compared to total LAI but ($r^2 = 0.36$, bias = -
18 0.043, and RMSE = 0.26). Accuracies decreased for the lowest canopy layers, with the r^2 values
19 falling from a peak of 0.66 at upper-story (15 to 20 m) to 0.33 at middle-story (5 to 10 m), to
20 essentially no relationship in the lowest 5 meters in the understory. There may be multiple factors
21 contributing to this trend. First, a slope effect may reduce measurement accuracy of GLAS (Tang
22 et al., 2014a). Slopes can blur the boundary between vegetation and topography signals in a lidar
23 waveform, making their separation difficult and potentially leading to the error in LAI and VFP
24 estimates. Despite methods to correct for topography (Lee et al., 2011; Tang et al., 2014a; Park et
25 al., 2014), this effect cannot be fully mitigated, especially over steep slopes, and consequently
26 may introduce errors and uncertainties into VFP estimates. Additionally, topographical effects
27 can lead to a vertical misalignment of VFP between LVIS and GLAS. GLAS measures the
28 terrestrial surface at a larger footprint with higher topographical variations, and a direct average
29 of LVIS VFP can possibly result in a mismatch of vertical foliage distribution up to several
30 meters. For example, consider two adjacent LVIS shots with the same VFP distribution but a 1 m

1 difference in ground elevation (like a signal lag in the waveform). Adding the two waveforms
2 along the geodetic altitude would lead to a 1 m vertical offset in the averaged waveform (pseudo-
3 GLAS waveform) and produce a different VFP using the direct average method in a normalized
4 coordinate system. But their total LAI values remain the same as long as the total energy from
5 ground and vegetation can be separately correctly. Reducing vertical resolution of VFP can
6 partially mitigate the mismatch effect because a lower vertical resolution requires integration over
7 longer vertical axis which is more tolerant to ground mismatch. Take the above example again,
8 the two VFP, at 1 m vertical resolution, do not match each other at all along the entire waveform
9 due to the offset. However, integration at every 5 m creates a signal overlap of 4 m in each height
10 bin with a maximum of 20% measurement error. Thus there is ultimately a tradeoff between
11 vertical resolution and VFP accuracy. It also explains the higher agreement of total LAI
12 (essentially an integration of VFP over the entire canopy) in the comparison between LVIS and
13 GLAS. Lastly, measurement of near-ground understory vegetation by GLAS is difficult. By
14 default GLAS waveforms are processed by a Gaussian decomposition method to get an
15 approximate fit comprised of a series of Gaussian functions where the last one usually represents
16 the ground (Hofton et al., 2000). The upper tail of the ground Gaussian peak may be mixed with
17 signals from lower understory, and their separation is problematic, especially over slopes. All of
18 these factors, plus the nature of high complexity and heterogeneity in canopy understory (Aubin
19 et al., 2000; Valladares and Niinemets, 2008), may help explain the lower agreement on
20 understory VFP between LVIS and GLAS.

21 Comparison between GLAS and Landsat displayed a much lower agreement than that of LVIS,
22 was somewhat biased, and showed clear signals of saturation beyond LAI values of about 5. This
23 result, along with all previous studies (Tang et al., 2012; Tang et al., 2014b), clearly showed the
24 non-saturation advantage of lidar data against passive remote sensing in observing high LAI
25 forests. On the low end of LAI spectrum, GLAS values were lower as compared with Landsat.
26 There are different factors (some in the LVIS comparison too) could possibly lead to their
27 difference in LAI estimates such as geolocation errors of GLAS shots, observation scale
28 difference (65 m vs. 30 m) and misclassifications from MODIS land cover types (mainly
29 impacting the correction of clumping effect). But this underestimation should be largely due to
30 the fact that GLAS may not be able to adequately capture LAI values of short grassland with

1 limited vertical structure or areas of sparse canopy cover, whereas Landsat is able measure such
2 areas based on their total spectral response (tree and grass).

3 Analysis of GLAS LAI and VFP across ecoregions displayed a reasonable and expected
4 geographical distribution. The great advantage of lidar based estimates is that they can produce
5 LAI vertical strata maps, providing a view of canopy variability across ecosystem types over
6 large areas. Specifically, we can identify the foliage concentrations at various vertical bins and at
7 spatial resolutions of interest (Fig. 6, Fig. 8 and Table 1; another example provided in the
8 supplement). This approach may reduce errors that arise from assumptions of uniformly
9 distributed foliage within canopy, and could potentially be a contribution towards continental
10 scale ecological and biological studies of forest structure and dynamics.

11 LAI and VFP also varied across different landscapes represented by various land cover types. As
12 expected, we found both total LAI and maximum value of foliage density significantly increase
13 along the vegetation gradient described by the transition from shrubland to savanna to woody
14 savanna to forests (Fig. 7 and Fig. 8). In particular, we found deciduous broadleaf forest showing
15 a different pattern with its foliage more evenly distributed in understory and mid-story when
16 compared with all other forests. Our results suggest the existence of canopy layering, and
17 highlight the feasibility of quantifying these layers across landscapes (Whitehurst et al., 2013).
18 Regardless, of whether the data are conceptualized as layers or as continuously varying profiles,
19 they nonetheless provide the actual vertical structure, and thus should help refine current
20 empirical assumptions about vegetation structure of different land cover types in current LAI
21 inversion algorithms (e.g. MODIS) and in ecosystem models (Hurtt et al., 2010; Antonarakis et
22 al., 2014).

23 Elevation and precipitation were found to be significantly correlated with LAI at both footprint
24 level and across aggregated groupings by elevation and forest ratio. LAI decreased with elevation
25 and this trend was consistent with previous studies (Luo et al., 2004; Moser et al., 2007; Pfeifer et
26 al., 2012). Variations of the trend can be largely explained (about 45 % of total variance) by the
27 Forest Ratio (defined in Sect. 3.3). A combination of the two factors (elevation groups and Forest
28 Ratio) explained almost 90% variance of average LAI spatial distribution. We also found a
29 significant but nonlinear relationship between GLAS LAI and annual precipitation (Fig. 10). This
30 non-linear relationship agrees with previous studies in the tropics (Pfeifer et al., 2014; Spracklen

1 et al., 2012). However, we found no significant variation of GLAS LAI with either temperature or
2 vapor pressure deficit variables. A combined effect of elevation and precipitation explains about
3 30% of LAI variation at GLAS footprint level, suggesting the natural complexity highly spatial
4 variability of LAI distribution.

5 As a direct quantification of 3D foliage distribution, GLAS LAI profiles are thus far the best
6 representations of terrestrial ecosystem structure over broad geographical areas and suggest that
7 ecological applications of these profiles are worth exploring. First, this data could refine large
8 scale modeling of plant respiration and photosynthesis and consequently and improve ecosystem
9 modeling (Houghton, 2007). Previous studies have reported a potential 50% underestimate of
10 GPP values when vertical foliage stratification is not considered (Kotchenova et al.,
11 2004;Sprintsin et al., 2012). A consistent, global data set of VFP should thus improve
12 initialization of ecological models (Hurtt et al., 2004), and refine estimation of GPP, in
13 conjunction with passive remote sensing data (Turner et al., 2006). Secondly, these profiles may
14 be important descriptors of habitat as related to biodiversity and habitat quality. Many studies
15 have confirmed the general relationship between species richness, habitat heterogeneity and
16 forest structural complexity across different landscapes (Swatantran et al., 2012;Goetz et al.,
17 2010;Schut et al., 2014;Fergner et al., 2014). The inclusion of LAI profiles provides spatially
18 explicit vegetation structure data and may potentially improve current observations of species
19 distribution at continental scale, e.g. for avian species (Sauer et al., 2008;Culbert et al., 2013), and
20 lead to entirely new biodiversity metrics (e.g. see (Huang et al., 2014)). For example the concept
21 of an "edge" has been traditionally defined as the boundary between forest and non-forest areas.
22 LAI profiles provide a means of defining new edges based on differences in LAI as a function of
23 height, so the edge is now the boundary between a rapid change in foliage density at a particular
24 height.

25

26 **5 Conclusion**

27 Accurate representation of canopy vertical structure and its dynamics has long been recognized as
28 a priority because it represents a key interface between terrestrial surface and atmosphere and
29 impacts the water and carbon cycles, and their transfer of energy and mass. Foliar profiles are

1 also increasingly recognized as important determinants for habitat quality, species distribution,
2 diversity and abundance. As ecosystems come under increasing pressure from climate and land
3 use change, global data sets of canopy structure are needed to help better understand the
4 consequences of these changes on ecosystem form, function and services.

5 In this paper we have demonstrated the potential for global mapping of key canopy structures,
6 LAI and VFP, from space. While imperfect, given their large footprint and sparse sampling, the
7 waveforms from ICESat are currently the only such global data set of structure. Our ability to
8 produce this data set is the end result of a series of research experiments that linked various types
9 of observations, from destructive profiles, to ground based optical methods, to airborne lidar, to
10 passive optical retrievals. This background gives us confidence that meaningful and useful data
11 on LAI and VFP can be derived from future spaceborne lidar. There are still hurdles to overcome
12 related to topography, understory accuracy, model assumptions and parameterizations, such as
13 ground/canopy reflectance ratios and foliage clumping, among others, to achieving higher
14 accuracy. We anticipate these will be resolved in time and lead to an even more capable model
15 suitable for the next generation of waveform lidar observations from space, such as NASA's
16 Global Ecosystem Dynamics Investigation (GEDI) (Dubayah et al., 2014) and potentially
17 ICESat-2 (Abdalati et al., 2009).

18

19 **Acknowledgements**

20 This work was funded by NASA under grant NNX12AK07G (Dubayah) and an Earth and Space
21 Science graduate fellowship NNX12AN43H (Dubayah/Tang). We thank Helen G. Cornejo and
22 Wenli Huang for raw LVIS waveform process, George Hurtt and Shunlin Liang for their advice
23 on product development. We also thank the NSIDC (National Snow & Ice Data Center) User
24 Services for their help on data acquisition and NASA Earth Exchange (NEX) for computing
25 resources.

1 **References**

- 2 Abdalati, W., Zwally, H. J., Bindschadler, R., Csatho, B., Farrell, S. L., Fricker, H. A., Harding,
3 D., Kwok, R., Lefsky, M., Markus, T., Marshak, A., Neumann, T., Palm, S., Schutz, B., Smith,
4 B., Spinhirne, J., and Webb, C.: The ICESat-2 laser altimetry mission, *Proceedings of the IEEE*,
5 98, 735-751, 2009.
- 6 Aber, J. D.: Foliage-height profiles and succession in northern hardwood forests, *Ecology*, 60,
7 18-23, 1979.
- 8 Abshire, J. B., Sun, X., Riris, H., Sirota, J. M., McGarry, J. F., Palm, S., Yi, D., and Liiva, P.:
9 Geoscience Laser Altimeter System (GLAS) on the icesat mission: On-orbit measurement
10 performance, *Geophysical Research Letters*, 32, L21S02, doi:10.1029/2005GL024028, 2005.
- 11 Abuelgasim, A. A., Fernandes, R. A., and Leblanc, S. G.: Evaluation of national and global lai
12 products derived from optical remote sensing instruments over canada, *IEEE Transactions on*
13 *Geoscience and Remote Sensing*, 44, 1872-1884, Doi 10.1109/Tgrs.2006.874794, 2006.
- 14 Antonarakis, A. S., Munger, J. W., and Moorcroft, P. R.: Imaging spectroscopy- and lidar-derived
15 estimates of canopy composition and structure to improve predictions of forest carbon fluxes and
16 ecosystem dynamics, *Geophysical Research Letters*, 41, 2535-2542, Doi 10.1002/2013gl058373,
17 2014.
- 18 Asner, G. P., Knapp, D. E., Boardman, J., Green, R. O., Kennedy-Bowdoin, T., Eastwood, M.,
19 Martin, R. E., Anderson, C., and Field, C. B.: Carnegie airborne observatory-2: Increasing
20 science data dimensionality via high-fidelity multi-sensor fusion, *Remote Sensing of*
21 *Environment*, 124, 454-465, DOI 10.1016/j.rse.2012.06.012, 2012.
- 22 Asner, G. P., Mascaro, J., Anderson, C., Knapp, D. E., Martin, R. E., Kennedy-Bowdoin, T., van
23 Breugel, M., Davies, S., Hall, J. S., Muller-Landau, H. C., Potvin, C., Sousa, W., Wright, J., and
24 Birmingham, E.: High-fidelity national carbon mapping for resource management and redd+,
25 *Carbon Balance and Management*, 8, 7, doi:10.1186/1750-0680-8-7, 2013.
- 26 Aubin, I., Beaudet, M., and Messier, C.: Light extinction coefficients specific to the understory
27 vegetation of the southern boreal forest, quebec, *Canadian Journal of Forest Research-Revue*
28 *Canadienne De Recherche Forestiere*, 30, 168-177, DOI 10.1139/cjfr-30-1-168, 2000.

1 Baccini, A., Goetz, S. J., Walker, W. S., Laporte, N. T., Sun, M., Sulla-Menashe, D., Hackler, J.,
2 Beck, P. S. A., Dubayah, R., Friedl, M. A., Samanta, S., and Houghton, R. A.: Estimated carbon
3 dioxide emissions from tropical deforestation improved by carbon-density maps, *Nature Climate*
4 *Change*, 2, 182-185, Doi 10.1038/Nclimate1354, 2012.

5 Baret, F., Hagolle, O., Geiger, B., Bicheron, P., Miras, B., Huc, M., Berthelot, B., Nino, F.,
6 Weiss, M., Samain, O., Roujean, J. L., and Leroy, M.: Lai, fapar and fcover cyclopes global
7 products derived from vegetation - part 1: Principles of the algorithm, *Remote Sensing of*
8 *Environment*, 110, 275-286, DOI 10.1016/j.rse.2007.02.018, 2007.

9 Baret, F., Weiss, M., Lacaze, R., Camacho, F., Makhmara, H., Pacholczyk, P., and Smets, B.:
10 Geov1: Lai and fapar essential climate variables and fcover global time series capitalizing over
11 existing products. Part1: Principles of development and production, *Remote Sensing of*
12 *Environment*, 137, 299-309, DOI 10.1016/j.rse.2012.12.027, 2013.

13 Blair, J. B., Rabine, D. L., and Hofton, M. A.: The laser vegetation imaging sensor (LVIS): A
14 medium-altitude, digitization-only, airborne laser altimeter for mapping vegetation and
15 topography, *ISPRS journal of photogrammetry and remote sensing*, 54, 115-122, 1999.

16 Brenner, A. C., Zwally, H. J., Bentley, C. R., Csatho, B. M., Harding, D. J., Hofton, M. A.,
17 Minster, J.-B., Roberts, L., Saba, J. L., and Thomas, R. H.: The algorithm theoretical basis
18 document for the derivation of range and range distributions from laser pulse waveform analysis
19 for surface elevations, roughness, slope, and vegetation heights, Goddard Space Flight Center,
20 Greenbelt, MD, United States, Technical Report NASA/TM-2012-208641/Vol 7,
21 GSFC.TM.7299.2012, 2012.

22 Chopping, M., Nolin, A., Moisen, G. G., Martonchik, J. V., and Bull, M.: Forest canopy height
23 from the multiangle imaging spectroradiometer (MISR) assessed with high resolution discrete
24 return lidar, *Remote Sensing of Environment*, 113, 2172-2185, DOI 10.1016/j.rse.2009.05.017,
25 2009.

26 Clark, D. B., and Kellner, J. R.: Tropical forest biomass estimation and the fallacy of misplaced
27 concreteness, *Journal of Vegetation Science*, 23, 1191-1196, DOI 10.1111/j.1654-
28 1103.2012.01471.x, 2012.

1 Cramer, W., Bondeau, A., Woodward, F. I., Prentice, I. C., Betts, R. A., Brovkin, V., Cox, P. M.,
2 Fisher, V., Foley, J. A., Friend, A. D., Kucharik, C., Lomas, M. R., Ramankutty, N., Sitch, S.,
3 Smith, B., White, A., and Young-Molling, C.: Global response of terrestrial ecosystem structure
4 and function to co₂ and climate change: Results from six dynamic global vegetation models,
5 *Global Change Biology*, 7, 357-373, DOI 10.1046/j.1365-2486.2001.00383.x, 2001.

6 Culbert, P. D., Radeloff, V. C., Flather, C. H., Kellndorfer, J. M., Rittenhouse, C. D., and
7 Pidgeon, A. M.: The influence of vertical and horizontal habitat structure on nationwide patterns
8 of avian biodiversity, *Auk*, 130, 656-665, DOI 10.1525/auk.2013.13007, 2013.

9 Deng, F., Chen, J. M., Plummer, S., Chen, M. Z., and Pisek, J.: Algorithm for global leaf area
10 index retrieval using satellite imagery, *IEEE Transactions on Geoscience and Remote Sensing*,
11 44, 2219-2229, Doi 10.1109/Tgrs.2006.872100, 2006.

12 Drake, J. B., Dubayah, R. O., Clark, D. B., Knox, R. G., Blair, J. B., Hofton, M. A., Chazdon, R.
13 L., Weishampel, J. F., and Prince, S. D.: Estimation of tropical forest structural characteristics
14 using large-footprint lidar, *Remote Sensing of Environment*, 79, 305-319, Doi 10.1016/S0034-
15 4257(01)00281-4, 2002.

16 Dubayah, R., Bergen, K., Hall, F., Hurtt, G., Houghton, R., Kellndorfer, J., Lefsky, M.,
17 Moorcroft, P., Nelson, R., and Saatchi, S.: Global vegetation structure from nasa's desdyni
18 mission: An overview, *AGU Fall Meeting Abstracts*, 01, San Francisco, 15 December, B31H- 01,
19 2008.

20 Dubayah, R., Goetz, S., Blair, J. B., Fatoyinbo, T., Hansen, M., Healey, S., Hofton, M., Hurtt, G.,
21 Kellner, J. R., Luthcke, S. B., and Swatantran, A.: The global ecosystem dynamics investigation,
22 *American Geophysical Union, Fall Meeting 2014*, San Francisco, 15 December, U14A-07, 2014.

23 Ferger, S. W., Schleuning, M., Hemp, A., Howell, K. M., and Böhning-Gaese, K.: Food resources
24 and vegetation structure mediate climatic effects on species richness of birds, *Global Ecology and*
25 *Biogeography*, 23, 541-549, 10.1111/geb.12151, 2014.

26 Friedl, M. A., Sulla-Menashe, D., Tan, B., Schneider, A., Ramankutty, N., Sibley, A., and Huang,
27 X. M.: Modis collection 5 global land cover: Algorithm refinements and characterization of new
28 datasets, *Remote Sensing of Environment*, 114, 168-182, DOI 10.1016/j.rse.2009.08.016, 2010.

1 Ganguly, S., et al. : Generating leaf area index from landsat over the Unites States. Manuscript in
2 preparation.

3 Ganguly, S., Nemani, R. R., Zhang, G., Hashimoto, H., Milesi, C., Michaelis, A., Wang, W. L.,
4 Votava, P., Samanta, A., Melton, F., Dungan, J. L., Vermote, E., Gao, F., Knyazikhin, Y., and
5 Myneni, R. B.: Generating global leaf area index from landsat: Algorithm formulation and
6 demonstration, *Remote Sensing of Environment*, 122, 185-202, DOI 10.1016/j.rse.2011.10.032,
7 2012.

8 Garcia, M., Popescu, S., Riano, D., Zhao, K., Neuenschwander, A., Agca, M., and Chuvieco, E.:
9 Characterization of canopy fuels using ICESat/GLAS data, *Remote Sensing of Environment*, 123,
10 81-89, 10.1016/j.rse.2012.03.018, 2012.

11 Goetz, S., Steinberg, D., Dubayah, R., and Blair, B.: Laser remote sensing of canopy habitat
12 heterogeneity as a predictor of bird species richness in an eastern temperate forest, USA, *Remote
13 Sensing of Environment*, 108, 254-263, DOI 10.1016/j.rse.2006.11.016, 2007.

14 Goetz, S. J., Steinberg, D., Betts, M. G., Holmes, R. T., Doran, P. J., Dubayah, R., and Hofton,
15 M.: Lidar remote sensing variables predict breeding habitat of a neotropical migrant bird,
16 *Ecology*, 91, 1569-1576, Doi 10.1890/09-1670.1, 2010.

17 Gower, S. T., and Norman, J. M.: Rapid estimation of leaf area index in conifer and broad-leaf
18 plantations, *Ecology*, 72, 1896-1900, 1991.

19 Harding, D. J., and Carabajal, C. C.: ICESat waveform measurements of within-footprint
20 topographic relief and vegetation vertical structure, *Geophysical Research Letters*, 32, Artn
21 L21s10, Doi 10.1029/2005gl023471, 2005.

22 Healey, S. P., Patterson, P. L., Saatchi, S., Lefsky, M. A., Lister, A. J., and Freeman, E. A.: A
23 sample design for globally consistent biomass estimation using lidar data from the Geoscience
24 Laser Altimeter System (GLAS), *Carbon Balance and Management*, 7, 10, doi:10.1186/1750-
25 0680-7-10, 2012.

26 Heimann, M., and Reichstein, M.: Terrestrial ecosystem carbon dynamics and climate feedbacks,
27 *Nature*, 451, 289-292, Doi 10.1038/Nature06591, 2008.

1 Hofton, M. A., Minster, J. B., and Blair, J. B.: Decomposition of laser altimeter waveforms, IEEE
2 Transactions on Geoscience and Remote Sensing, 38, 1989-1996, 2000.

3 Houghton, R. A.: Balancing the global carbon budget, Annual Review of Earth and Planetary
4 Sciences, 35, 313-347, DOI 10.1146/annurev.earth.35.031306.140057, 2007.

5 Huang, Q. Y., Swatantran, A., Dubayah, R., and Goetz, S. J.: The influence of vegetation height
6 heterogeneity on forest and woodland bird species richness across the united states, Plos One, 9,
7 ARTN e103236, DOI 10.1371/journal.pone.0103236, 2014.

8 Hurtt, G. C., Dubayah, R., Drake, J., Moorcroft, P. R., Pacala, S. W., Blair, J. B., and Fearon, M.
9 G.: Beyond potential vegetation: Combining lidar data and a height-structured model for carbon
10 studies, Ecological Applications, 14, 873-883, 2004.

11 Hurtt, G. C., Fisk, J., Thomas, R. Q., Dubayah, R., Moorcroft, P. R., and Shugart, H. H.: Linking
12 models and data on vegetation structure, Journal of Geophysical Research-Biogeosciences, 115,
13 Artn G00e10, Doi 10.1029/2009jg000937, 2010.

14 Kotchenova, S. Y., Song, X. D., Shabanova, N. V., Potter, C. S., Knyazikhin, Y., and Myneni, R.
15 B.: Lidar remote sensing for modeling gross primary production of deciduous forests, Remote
16 Sensing of Environment, 92, 158–172, doi:10.1016/j.rse.2004.05.010, 2004.

17 Lee, S., Ni-Meister, W., Yang, W. Z., and Chen, Q.: Physically based vertical vegetation
18 structure retrieval from icesat data: Validation using LVIS in white mountain national forest, new
19 hampshire, USA, Remote Sensing of Environment, 115, 2776-2785, DOI
20 10.1016/j.rse.2010.08.026, 2011.

21 Lefsky, M. A., Cohen, W. B., Parker, G. G., and Harding, D. J.: Lidar remote sensing for
22 ecosystem studies, BioScience, 52, 19-19, 2002.

23 Lefsky, M. A.: A global forest canopy height map from the moderate resolution imaging
24 spectroradiometer and the geoscience laser altimeter system, Geophysical Research Letters, 37,
25 L15401, doi:10.1029/2010GL043622, 2010.

26 Loreau, M., Naeem, S., Inchausti, P., Bengtsson, J., Grime, J. P., Hector, A., Hooper, D. U.,
27 Huston, M. A., Raffaelli, D., Schmid, B., Tilman, D., and Wardle, D. A.: Ecology - biodiversity

1 and ecosystem functioning: Current knowledge and future challenges, *Science*, 294, 804-808,
2 DOI 10.1126/science.1064088, 2001.

3 Los, S. O., Rosette, J. A. B., Kljun, N., North, P. R. J., Chasmer, L., Suñez, J. C., Hopkinson,
4 C., Hill, R. A., van Gorsel, E., Mahoney, C., and Berni, J. A. J.: Vegetation height and cover
5 fraction between 60° s and 60° n from ICESat GLAS data, *Geosci. Model Dev.*, 5, 413-432,
6 10.5194/gmd-5-413-2012, 2012.

7 Luo, S. Z., Wang, C., Li, G. C., and Xi, X. H.: Retrieving leaf area index using icesat/glas full-
8 waveform data, *Remote Sensing Letters*, 4, 745-753, Doi 10.1080/2150704x.2013.790573, 2013.

9 Luo, T. X., Pan, Y. D., Ouyang, H., Shi, P. L., Luo, J., Yu, Z. L., and Lu, Q.: Leaf area index and
10 net primary productivity along subtropical to alpine gradients in the tibetan plateau, *Global
11 Ecology and Biogeography*, 13, 345-358, DOI 10.1111/j.1466-822X.2004.00094.x, 2004.

12 Morsdorf, F., Kotz, B., Meier, E., Itten, K., and Allgower, B.: Estimation of lai and fractional
13 cover from small footprint airborne laser scanning data based on gap fraction, *Remote Sensing of
14 Environment*, 104, 50-61, 2006.

15 Moser, G., Hertel, D., and Leuschner, C.: Altitudinal change in lai and stand leaf biomass in
16 tropical montane forests: A transect shady in ecuador and a pan-tropical meta-analysis,
17 *Ecosystems*, 10, 924-935, DOI 10.1007/s10021-007-9063-6, 2007.

18 Mu, Q., Heinsch, F. A., Zhao, M., and Running, S. W.: Development of a global
19 evapotranspiration algorithm based on modis and global meteorology data, *Remote Sensing of
20 Environment*, 111, 519-536, DOI 10.1016/j.rse.2007.04.015, 2007.

21 Myneni, R. B., Hoffman, S., Knyazikhin, Y., Privette, J. L., Glassy, J., Tian, Y., Wang, Y., Song,
22 X., Zhang, Y., Smith, G. R., Lotsch, A., Friedl, M., Morisette, J. T., Votava, P., Nemani, R. R.,
23 and Running, S. W.: Global products of vegetation leaf area and fraction absorbed par from year
24 one of modis data, *Remote Sensing of Environment*, 83, 214-231, Pii S0034-4257(02)00074-3
25 Doi 10.1016/S0034-4257(02)00074-3, 2002.

26 Ni-Meister, W., Jupp, D. L. B., and Dubayah, R.: Modeling lidar waveforms in heterogeneous
27 and discrete canopies, *IEEE Transactions on Geoscience and Remote Sensing*, 39, 1943-1958,
28 2001.

1 Nilson, T.: A theoretical analysis of the frequency of gaps in plant stands, *Agricultural*
2 *Meteorology*, 8, 25-38, 1971.

3 Olson, D. M., Dinerstein, E., Wikramanayake, E. D., Burgess, N. D., Powell, G. V. N.,
4 Underwood, E. C., D'amico, J. A., Itoua, I., Strand, H. E., Morrison, J. C., Loucks, C. J., Allnutt,
5 T. F., Ricketts, T. H., Kura, Y., Lamoreux, J. F., Wettengel, W. W., Hedao, P., and Kassem, K.
6 R.: Terrestrial ecoregions of the world: A new map of life on earth: A new global map of
7 terrestrial ecoregions provides an innovative tool for conserving biodiversity, *BioScience*, 51,
8 933-938, 10.1641/0006-3568(2001)051[0933:teotwa]2.0.co;2, 2001.

9 Park, T., Kennedy, R. E., Choi, S. H., Wu, J. W., Lefsky, M. A., Bi, J., Mantooth, J. A., Myneni,
10 R. B., and Knyazikhin, Y.: Application of physically-based slope correction for maximum forest
11 canopy height estimation using waveform lidar across different footprint sizes and locations:
12 Tests on lvis and glas, *Remote Sensing*, 6, 6566-6586, Doi 10.3390/Rs6076566, 2014.

13 Pereira, H. M., Ferrier, S., Walters, M., Geller, G. N., Jongman, R. H. G., Scholes, R. J., Bruford,
14 M. W., Brummitt, N., Butchart, S. H. M., Cardoso, A. C., Coops, N. C., Dulloo, E., Faith, D. P.,
15 Freyhof, J., Gregory, R. D., Heip, C., Hoft, R., Hurtt, G., Jetz, W., Karp, D. S., McGeoch, M. A.,
16 Obura, D., Onoda, Y., Pettorelli, N., Reyers, B., Sayre, R., Scharlemann, J. P. W., Stuart, S. N.,
17 Turak, E., Walpole, M., and Wegmann, M.: Essential biodiversity variables, *Science*, 339, 277-
18 278, DOI 10.1126/science.1229931, 2013.

19 Pfeifer, M., Gonsamo, A., Disney, M., Pellikka, P., and Marchant, R.: Leaf area index for biomes
20 of the eastern arc mountains: Landsat and spot observations along precipitation and altitude
21 gradients, *Remote Sensing of Environment*, 118, 103-115, DOI 10.1016/j.rse.2011.11.009, 2012.

22 Pfeifer, M., Lefebvre, V., Gonsamo, A., Pellikka, P., Marchant, R., Denu, D., and Platts, P.:
23 Validating and linking the gimms leaf area index (LAI3g) with environmental controls in tropical
24 africa, *Remote Sensing*, 6, 1973-1990, 2014.

25 PRISM: 30 yr normal precipitation: annual, in: 1981–2010, August 2013 ed., PRISM Climate
26 Group, Oregon State University, Corvallis, OR, 2013.

27 Randerson, J. T., Hoffman, F. M., Thornton, P. E., Mahowald, N. M., Lindsay, K., Lee, Y. H.,
28 Nevison, C. D., Doney, S. C., Bonan, G., Stockli, R., Covey, C., Running, S. W., and Fung, I. Y.:

1 Systematic assessment of terrestrial biogeochemistry in coupled climate-carbon models, *Global*
2 *Change Biology*, 15, 2462-2484, DOI 10.1111/j.1365-2486.2009.01912.x, 2009.

3 Reuter, H. I., Nelson, A., and Jarvis, A.: An evaluation of void-filling interpolation methods for
4 srtm data, *International Journal of Geographical Information Science*, 21, 983-1008, Doi
5 10.1080/13658810601169899, 2007.

6 Saatchi, S. S., Harris, N. L., Brown, S., Lefsky, M., Mitchard, E. T. A., Salas, W., Zutta, B. R.,
7 Buermann, W., Lewis, S. L., Hagen, S., Petrova, S., White, L., Silman, M., and Morel, A.:
8 Benchmark map of forest carbon stocks in tropical regions across three continents, *Proceedings*
9 *of the National Academy of Sciences of the United States of America*, 108, 9899-9904, DOI
10 10.1073/pnas.1019576108, 2011.

11 Sauer, J. R., Hines, J. E., Fallon, J., Pardieck, K., Ziolkowski Jr, D., and Link, W.: The north
12 american breeding bird survey, results and analysis 1966-2007, Version, 5, Laurel, MD, USGS
13 Patuxent Wildlife Research Center, 2008.

14 Schimel, D. S., House, J. I., Hibbard, K. A., Bousquet, P., Ciais, P., Peylin, P., Braswell, B. H.,
15 Apps, M. J., Baker, D., Bondeau, A., Canadell, J., Churkina, G., Cramer, W., Denning, A. S.,
16 Field, C. B., Friedlingstein, P., Goodale, C., Heimann, M., Houghton, R. A., Melillo, J. M.,
17 Moore, B., Murdiyarso, D., Noble, I., Pacala, S. W., Prentice, I. C., Raupach, M. R., Rayner, P.
18 J., Scholes, R. J., Steffen, W. L., and Wirth, C.: Recent patterns and mechanisms of carbon
19 exchange by terrestrial ecosystems, *Nature*, 414, 169-172, Doi 10.1038/35102500, 2001.

20 Schut, A. G. T., Wardell-Johnson, G. W., Yates, C. J., Keppel, G., Baran, I., Franklin, S. E.,
21 Hopper, S. D., Van Niel, K. P., Mucina, L., and Byrne, M.: Rapid characterisation of vegetation
22 structure to predict refugia and climate change impacts across a global biodiversity hotspot, *Plos*
23 *One*, 9, ARTN e82778, DOI 10.1371/journal.pone.0082778, 2014.

24 Shabanov, N. V., Huang, D., Yang, W. Z., Tan, B., Knyazikhin, Y., Myneni, R. B., Ahl, D. E.,
25 Gower, S. T., Huete, A. R., Aragao, L. E. O. C., and Shimabukuro, Y. E.: Analysis and
26 optimization of the modis leaf area index algorithm retrievals over broadleaf forests, *IEEE*
27 *Transactions on Geoscience and Remote Sensing*, 43, 1855-1865, Doi
28 10.1109/Tgrs.2005.852477, 2005.

1 Simard, M., Pinto, N., Fisher, J. B., and Baccini, A.: Mapping forest canopy height globally with
2 spaceborne lidar, *Journal of Geophysical Research-Biogeosciences*, 116, Artn G04021, Doi
3 10.1029/2011jg001708, 2011.

4 Spracklen, D. V., Arnold, S. R., and Taylor, C. M.: Observations of increased tropical rainfall
5 preceded by air passage over forests, *Nature*, 489, 282-U127, Doi 10.1038/Nature11390, 2012.

6 Sprintsin, M., Chen, J. M., Desai, A., and Gough, C. M.: Evaluation of leaf-to-canopy upscaling
7 methodologies against carbon flux data in north america, *Journal of Geophysical Research-*
8 *Biogeosciences*, 117, Artn G01023, Doi 10.1029/2010jg001407, 2012.

9 Stahl, G., Holm, S., Gregoire, T. G., Gobakken, T., Naesset, E., and Nelson, R.: Model-based
10 inference for biomass estimation in a lidar sample survey in hedmark county, norway, *Canadian*
11 *Journal of Forest Research-Revue Canadienne De Recherche Forestiere*, 41, 96-107, Doi
12 10.1139/X10-161, 2011.

13 Strahler, A. H., Jupp, D. L. B., Woodcock, C. E., Schaaf, C. B., Yao, T., Zhao, F., Yang, X.,
14 Lovell, J., Culvenor, D., Newnham, G., Ni-Miester, W., and Boykin-Morris, W.: Retrieval of
15 forest structural parameters using a ground-based lidar instrument (echidna®), *Canadian Journal*
16 *of Remote Sensing*, 34, S426–S440, doi:10.5589/m08-046, 2008.

17 Swatantran, A., Dubayah, R., Goetz, S., Hofton, M., Betts, M. G., Sun, M., Simard, M., and
18 Holmes, R.: Mapping migratory bird prevalence using remote sensing data fusion, *Plos One*, 7,
19 e28922, doi:10.1371/journal.pone.0028922, 2012.

20 Tang, H., Dubayah, R., Swatantran, A., Hofton, M., Sheldon, S., Clark, D. B., and Blair, B.:
21 Retrieval of vertical lai profiles over tropical rain forests using waveform lidar at la selva, costa
22 rica, *Remote Sensing of Environment*, 124, 242-250, 10.1016/j.rse.2012.05.005, 2012.

23 Tang, H., Brolly, M., Zhao, F., Strahler, A. H., Schaaf, C. L., Ganguly, S., Zhang, G., and
24 Dubayah, R.: Deriving and validating leaf area index (lai) at multiple spatial scales through lidar
25 remote sensing: A case study in sierra national forest, ca, *Remote Sensing of Environment*, 143,
26 131-141, 2014a.

1 Tang, H., Dubayah, R., Brolly, M., Ganguly, S., and Zhang, G.: Large-scale retrieval of leaf area
2 index and vertical foliage profile from the spaceborne waveform lidar (glas/icesat), *Remote
3 Sensing of Environment*, 154, 8-18, DOI 10.1016/j.rse.2014.08.007, 2014b.

4 Turner, D. P., Ritts, W. D., Cohen, W. B., Gower, S. T., Running, S. W., Zhao, M. S., Costa, M.
5 H., Kirschbaum, A. A., Ham, J. M., Saleska, S. R., and Ahl, D. E.: Evaluation of modis npp and
6 gpp products across multiple biomes, *Remote Sensing of Environment*, 102, 282-292, DOI
7 10.1016/j.rse.2006.02.017, 2006.

8 Turner, W., Spector, S., Gardiner, N., Fladeland, M., Sterling, E., and Steininger, M.: Remote
9 sensing for biodiversity science and conservation, *Trends in Ecology & Evolution*, 18, 306-314,
10 Doi 10.1016/S0169-5347(03)00070-3, 2003.

11 Valladares, F., and Niinemets, U.: Shade tolerance, a key plant feature of complex nature and
12 consequences, *Annual Review of Ecology Evolution and Systematics*, 39, 237-257, DOI
13 10.1146/annurev.ecolsys.39.110707.173506, 2008.

14 Whitehurst, A. S., Swatantran, A., Blair, J. B., Hofton, M. A., and Dubayah, R.: Characterization
15 of canopy layering in forested ecosystems using full waveform lidar, *Remote Sensing*, 5, 2014-
16 2036, Doi 10.3390/Rs5042014, 2013.

17 Yang, W. Z., Tan, B., Huang, D., Rautiainen, M., Shabanov, N. V., Wang, Y., Privette, J. L.,
18 Huemmrich, K. F., Fensholt, R., Sandholt, I., Weiss, M., Ahl, D. E., Gower, S. T., Nemani, R. R.,
19 Knyazikhin, Y., and Myneni, R. B.: Modis leaf area index products: From validation to algorithm
20 improvement, *IEEE Transactions on Geoscience and Remote Sensing*, 44, 1885-1898, Doi
21 10.1109/Tgrs.2006.871215, 2006.

22 Zhao, F., Yang, X. Y., Strahler, A. H., Schaaf, C. L., Yao, T., Wang, Z. S., Roman, M. O.,
23 Woodcock, C. E., Ni-Meister, W., Jupp, D. L. B., Lovell, J. L., Culvenor, D. S., Newnham, G. J.,
24 Tang, H., and Dubayah, R. O.: A comparison of foliage profiles in the sierra national forest
25 obtained with a full-waveform under-canopy evi lidar system with the foliage profiles obtained
26 with an airborne full-waveform lvis lidar system, *Remote Sensing of Environment*, 136, 330-341,
27 DOI 10.1016/j.rse.2013.05.020, 2013.

1 Zhao, M. S., Heinsch, F. A., Nemani, R. R., and Running, S. W.: Improvements of the modis
2 terrestrial gross and net primary production global data set, *Remote Sensing of Environment*, 95,
3 164-176, DOI 10.1016/j.rse.2004.12.011, 2005.

4

5

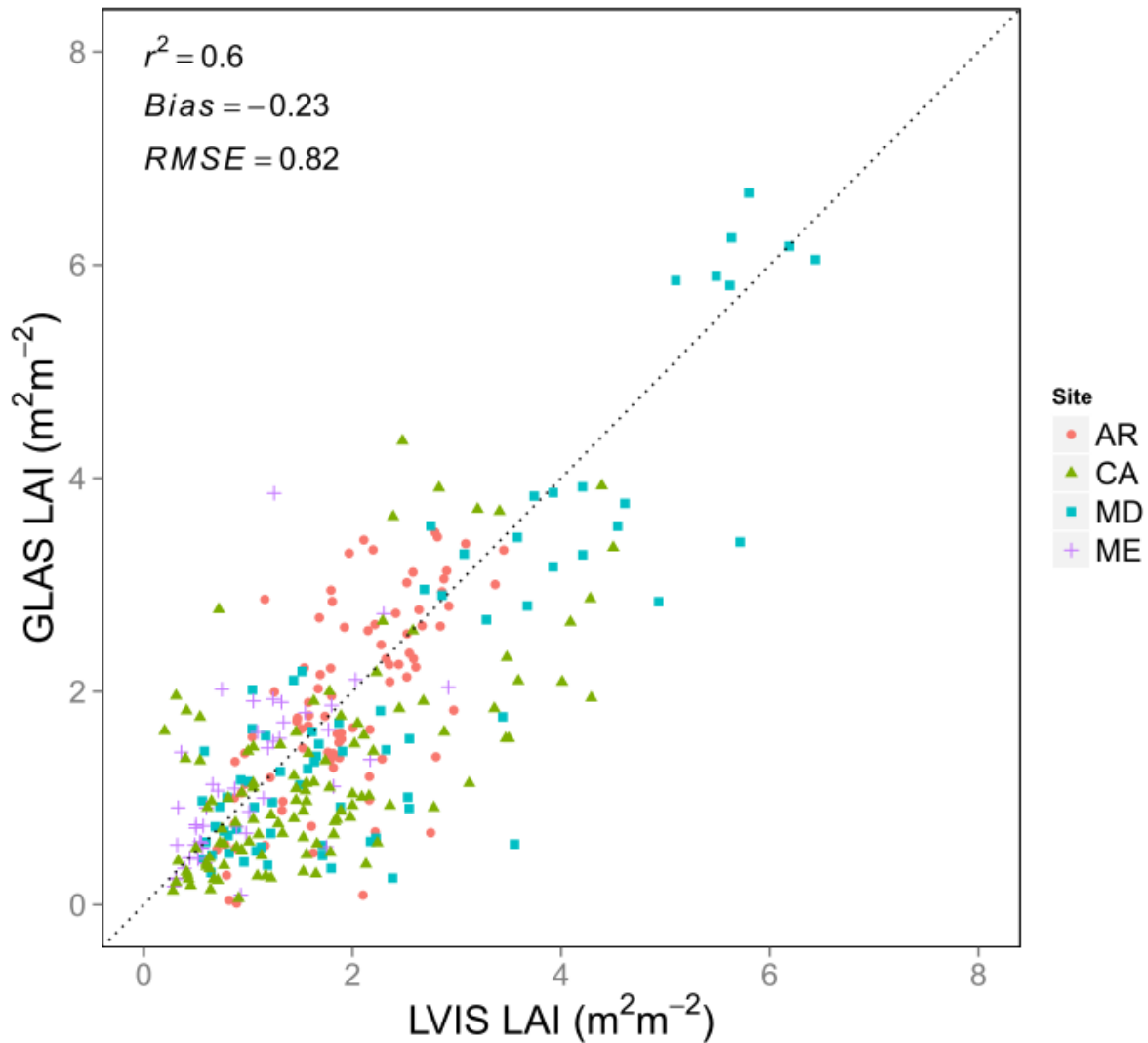
6

1 Table 1 Ecoregions with highest total LAI values (unit: $m^2 m^{-2}$)

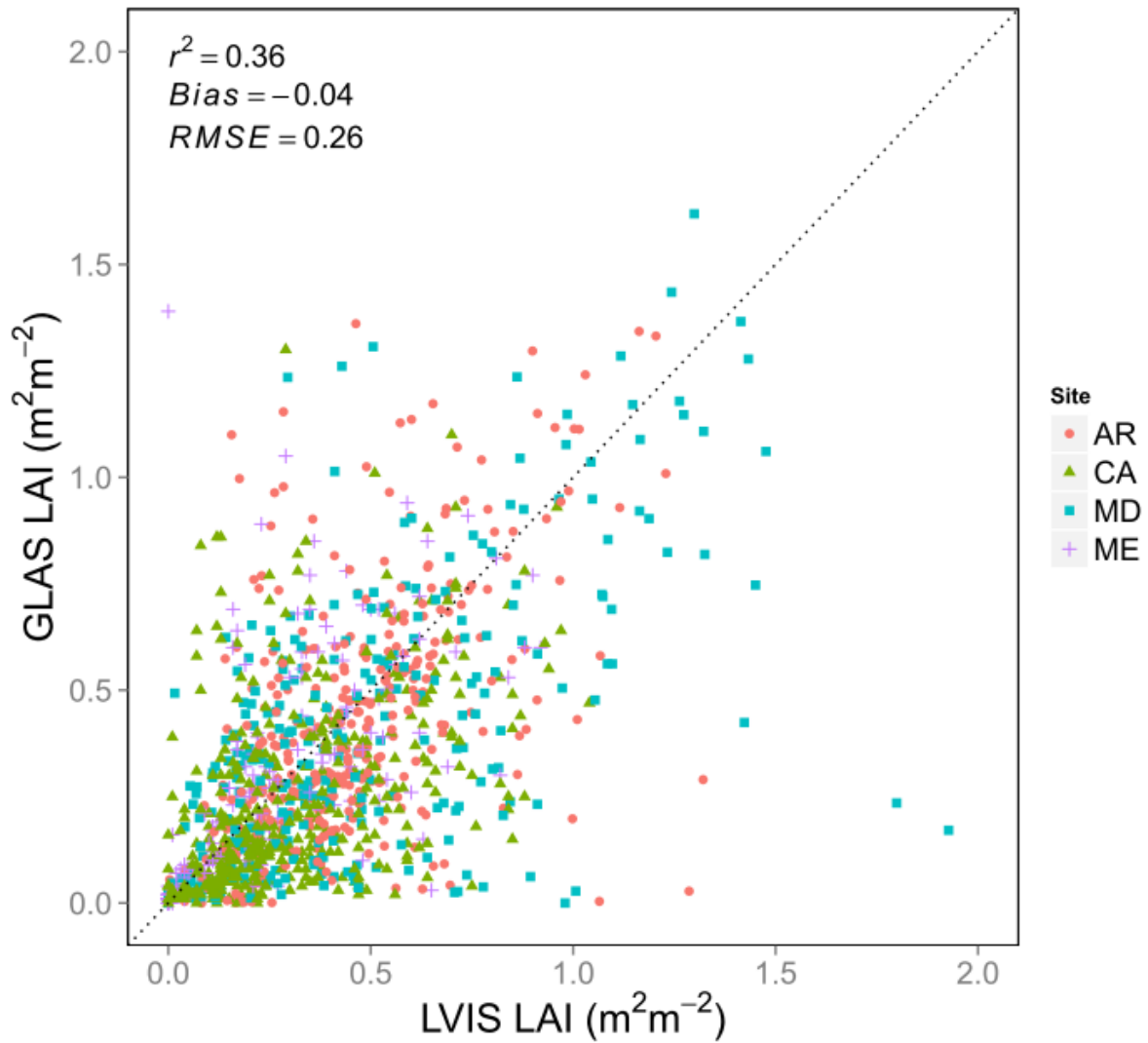
Ecoregions	Total LAI Mean(\pm SD)	LAI 0-10m Mean(\pm SD)	LAI 10-20m Mean(\pm SD)	LAI >20m Mean(\pm SD)
Northern California coastal forests	5.24 \pm 2.11	2.06 \pm 1.32	1.67 \pm 1.09	1.08 \pm 1.15
Central Pacific coastal forests	5.00 \pm 2.14	1.52 \pm 1.61	1.10 \pm 1.16	0.84 \pm 1.25
British Columbia mainland coastal forests	4.74 \pm 2.26	1.48 \pm 1.31	1.23 \pm 1.08	1.13 \pm 1.13
Central and Southern Cascades forests	4.31 \pm 2.34	1.06 \pm 1.35	0.79 \pm 1.02	0.64 \pm 1.07
Klamath-Siskiyou forests	4.31 \pm 2.31	1.26 \pm 1.30	0.99 \pm 1.07	0.73 \pm 0.99
Willamette Valley forests	3.99 \pm 2.24	0.73 \pm 1.09	0.60 \pm 0.89	0.75 \pm 1.31
Appalachian-Blue Ridge forests	3.95 \pm 2.03	1.04 \pm 1.27	0.82 \pm 0.99	0.47 \pm 0.82
Puget lowland forests	3.91 \pm 2.25	0.98 \pm 1.39	0.71 \pm 1.08	0.40 \pm 0.81
Appalachian mixed mesophytic forests	3.86 \pm 2.04	1.06 \pm 1.29	0.77 \pm 0.93	0.48 \pm 0.83
North Central Rockies forests	3.67 \pm 2.27	1.61 \pm 1.55	0.84 \pm 0.89	0.47 \pm 0.72

2

3



1
 2 Fig. 1 A comparison between two lidar derived Leaf Area Index (LAI) datasets at different sites
 3 across the US (N = 318), produced from the Laser Vegetation Imaging Sensor (LVIS) and the
 4 Geoscience Laser Altimeter System (GLAS) respectively. Each point represents a comparison at
 5 GLAS footprint while different colors and shapes indicate different sites (AR: White River
 6 National Wildlife Refuge in Arkansas; CA: Sierra National Forest in California; MD:
 7 Baltimore/Washington corridor in Maryland; ME: Maine forests to the north of Orono, Maine).
 8 The comparison produces r^2 of 0.60, bias of -0.23, and RMSE of 0.82). Dashed line is the 1:1 line.
 9

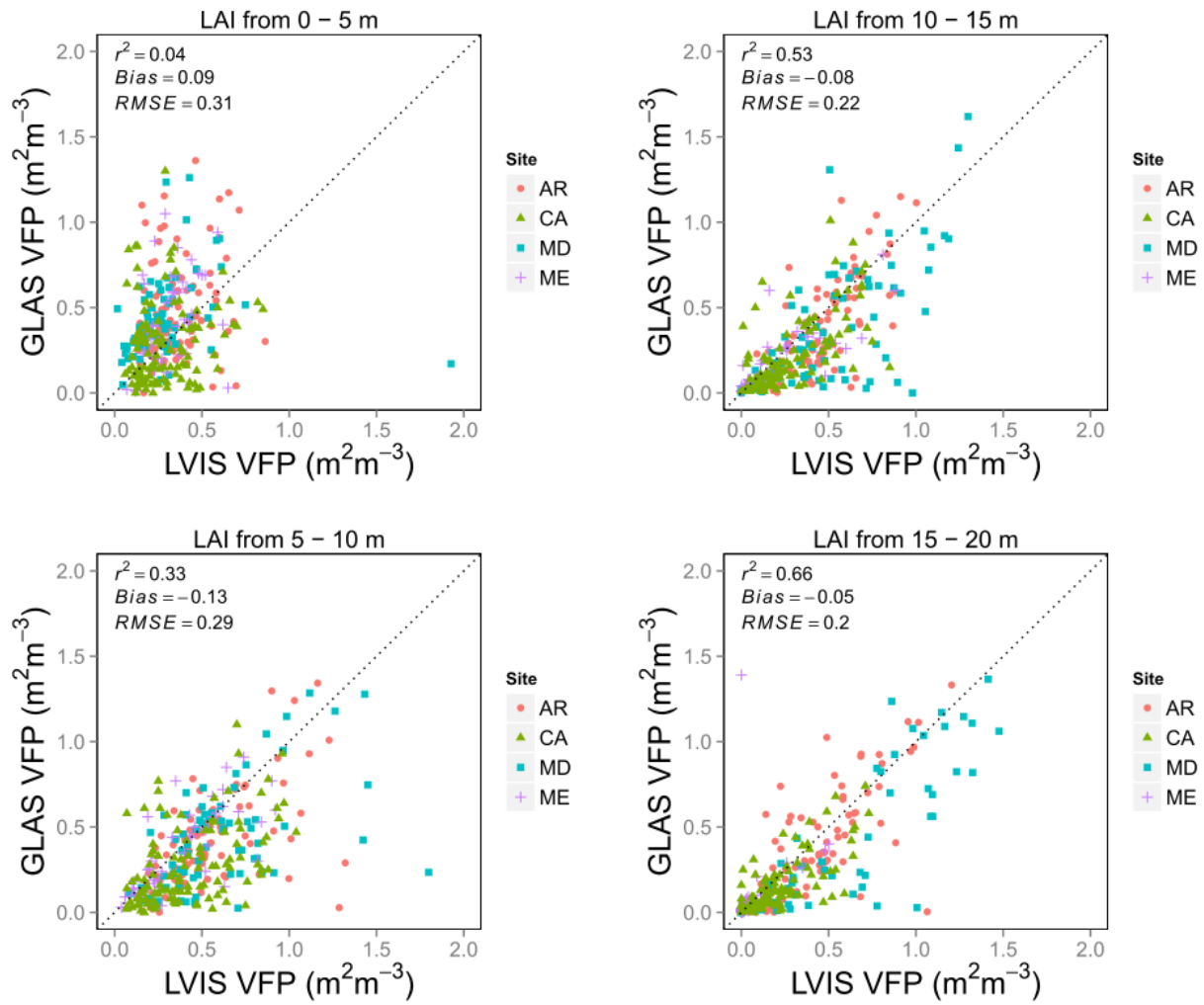


1

2 Fig. 2 A comparison of Vertical Foliage Profile (VFP) density derived from LVIS and GLAS

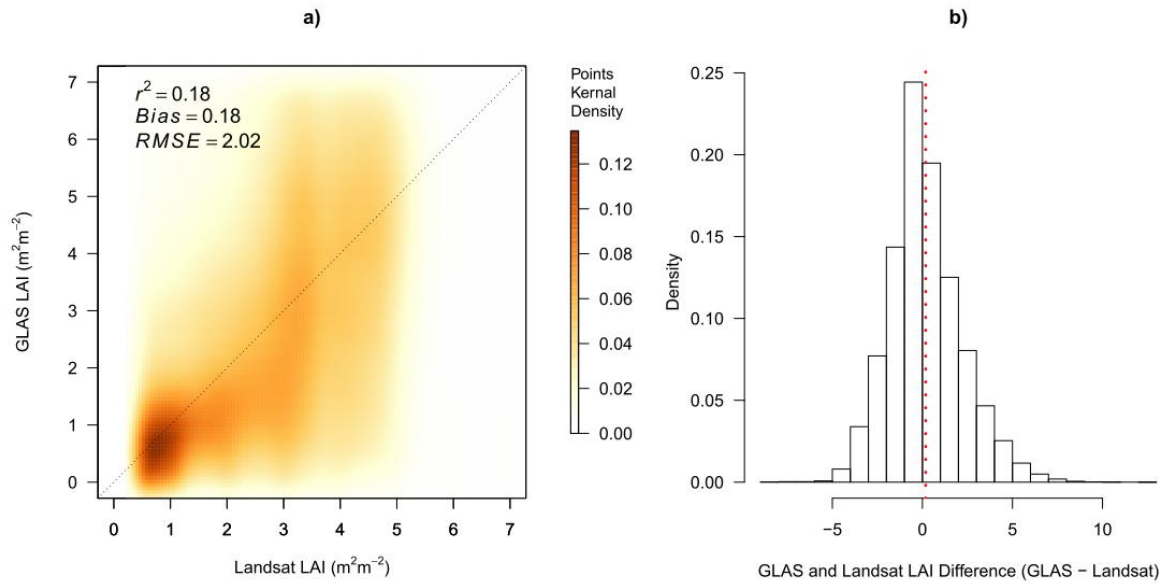
3 over different sites in the US (same sites as Fig.1 but with $N = 1272$). Each VFP point represents

4 an integrated value of foliage density at each 5 m height interval.



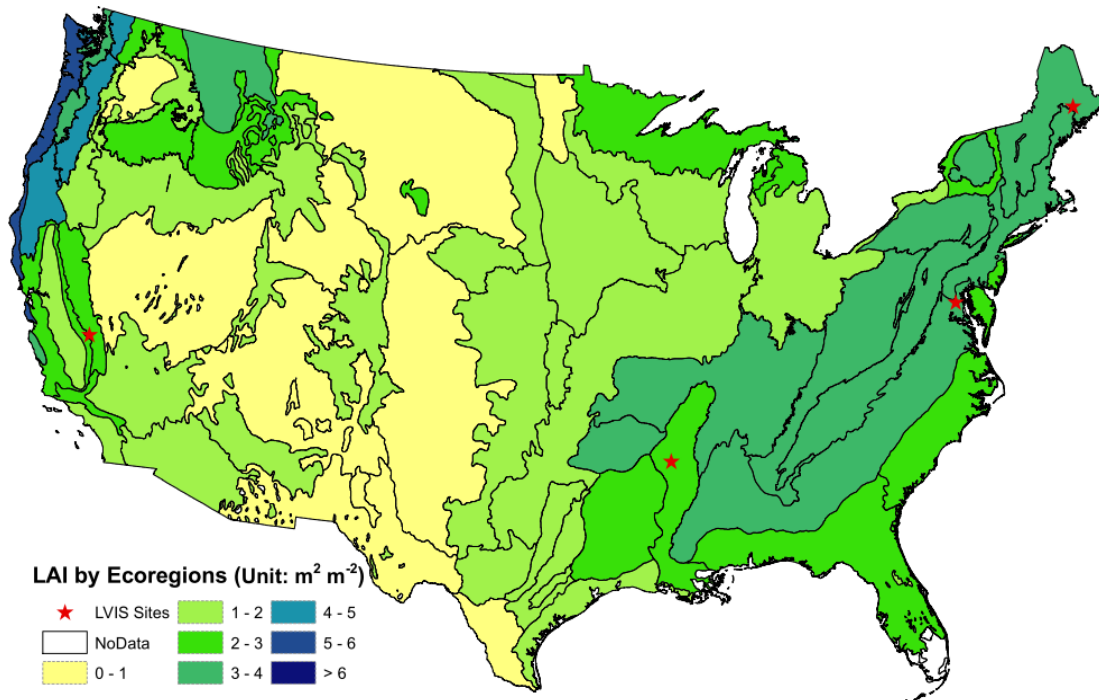
1
2

3 Fig. 3 Comparison between LVIS and GLAS VFP density integrated at every 5 m height interval
4 (from ground to canopy top).



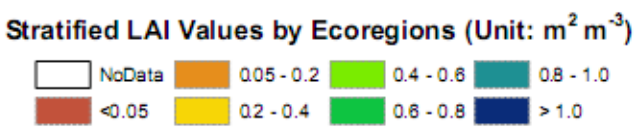
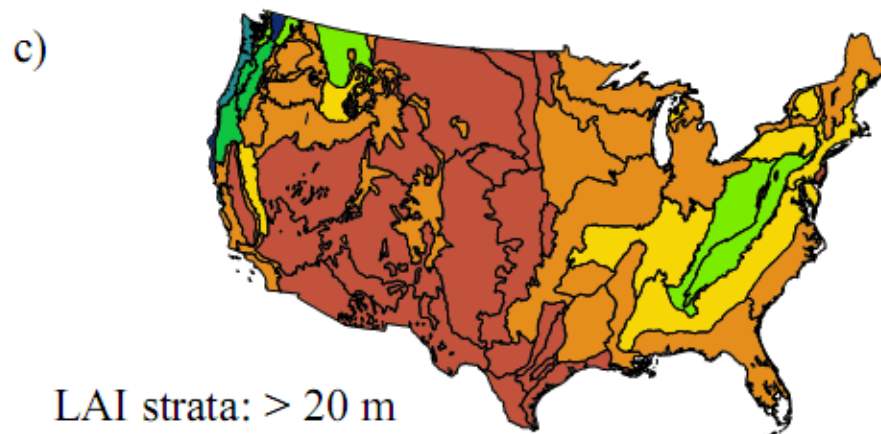
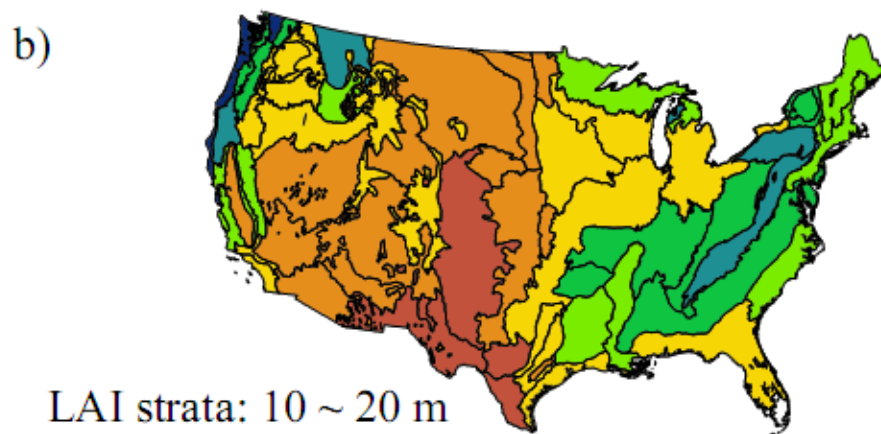
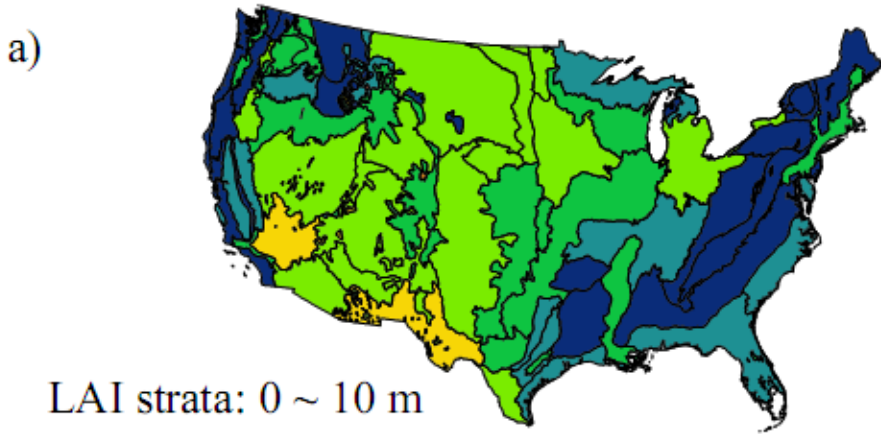
1
2

3 Fig. 4 Comparison between Landsat LAI and GLAS LAI over contiguous US: a) density scatter
 4 plot of Landsat and GLAS LAI ($r^2 = 0.18$, bias = 0.18 and RMSE = 2.02); b) Difference between
 5 Landsat and GLAS LAI. Darker kernel density color refers to more clustered distribution of LAI
 6 pairs.



1
2

3 Fig. 5 GLAS LAI distributions by ecoregion. All LVIS sites are marked with red stars.

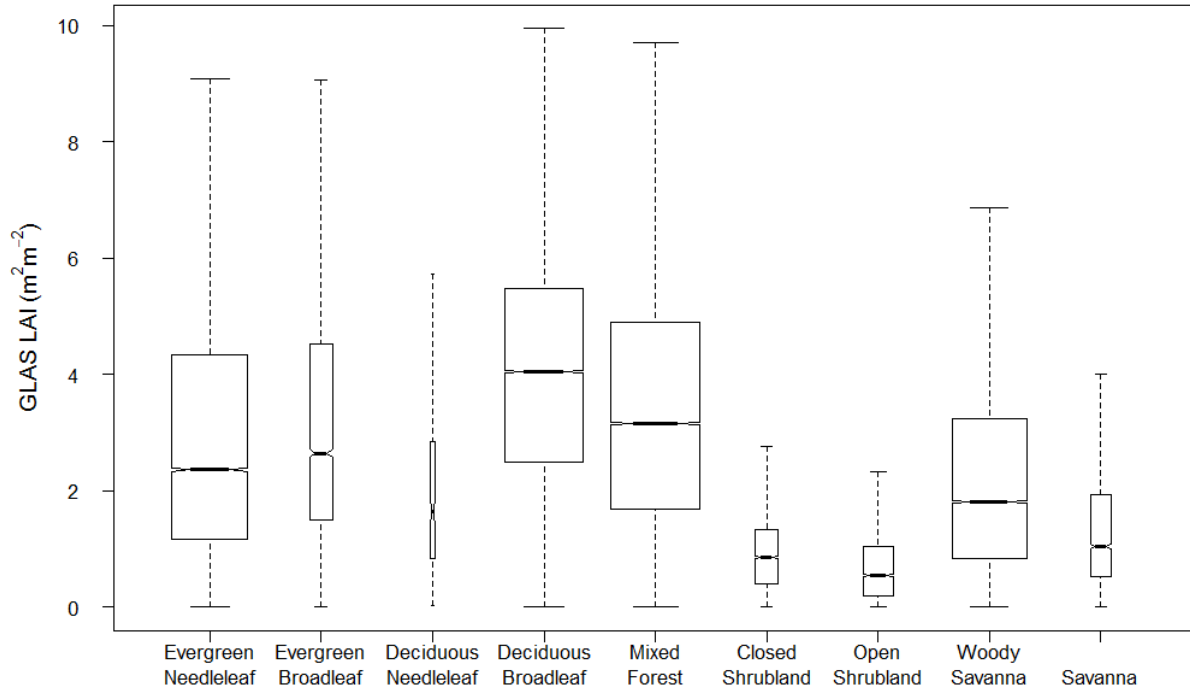


1

2

3

Fig. 6 LAI strata distributions by WWF ecoregions. Despite similar total LAI values, the southeastern forests show different LAI values at stratified height intervals.



1

2 Fig. 7 Distribution of total GLAS LAI across different land cover types. The width of the boxes is

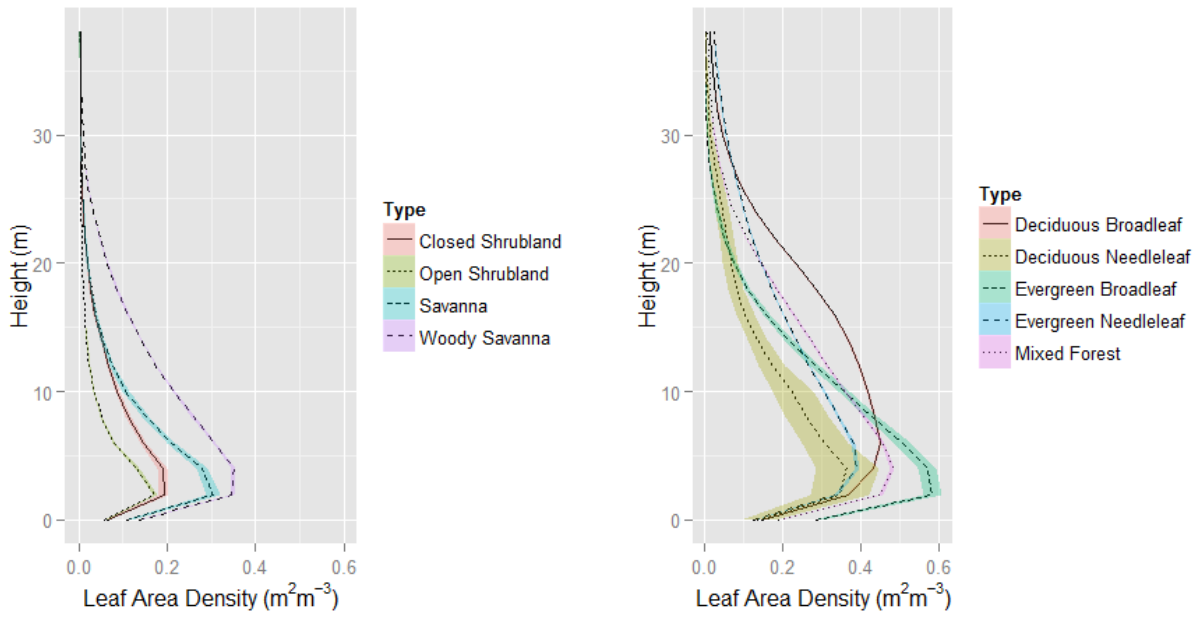
3 proportional to the number of observations for each type (N = Evergreen Needleleaf: 45207,

4 Evergreen Broadleaf: 438, Deciduous Needleleaf: 123, Deciduous Broadleaf: 48283, Mixed

5 Forest: 62053, Closed Shrubland: 4087, Open Shrubland: 7364, Woody Savanna: 43536,

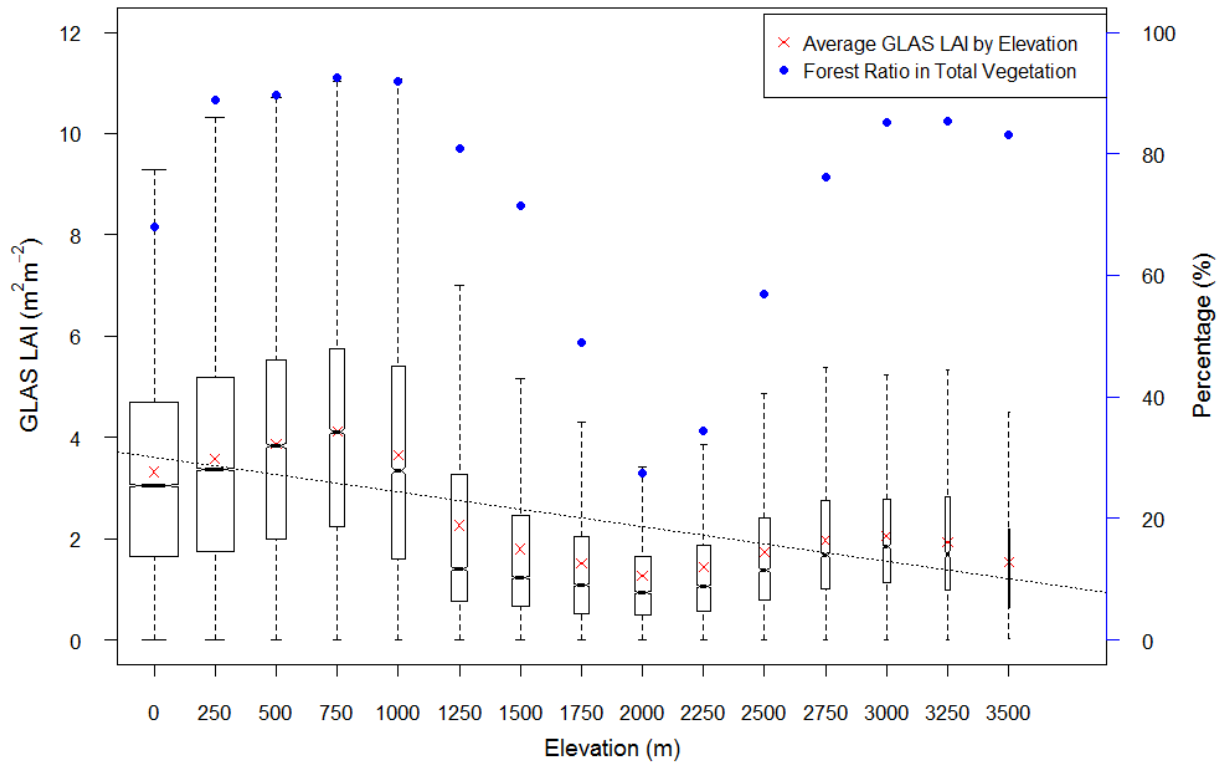
6 Savanna: 3051). Notches show the approximate 95% confidence interval of the median.

7

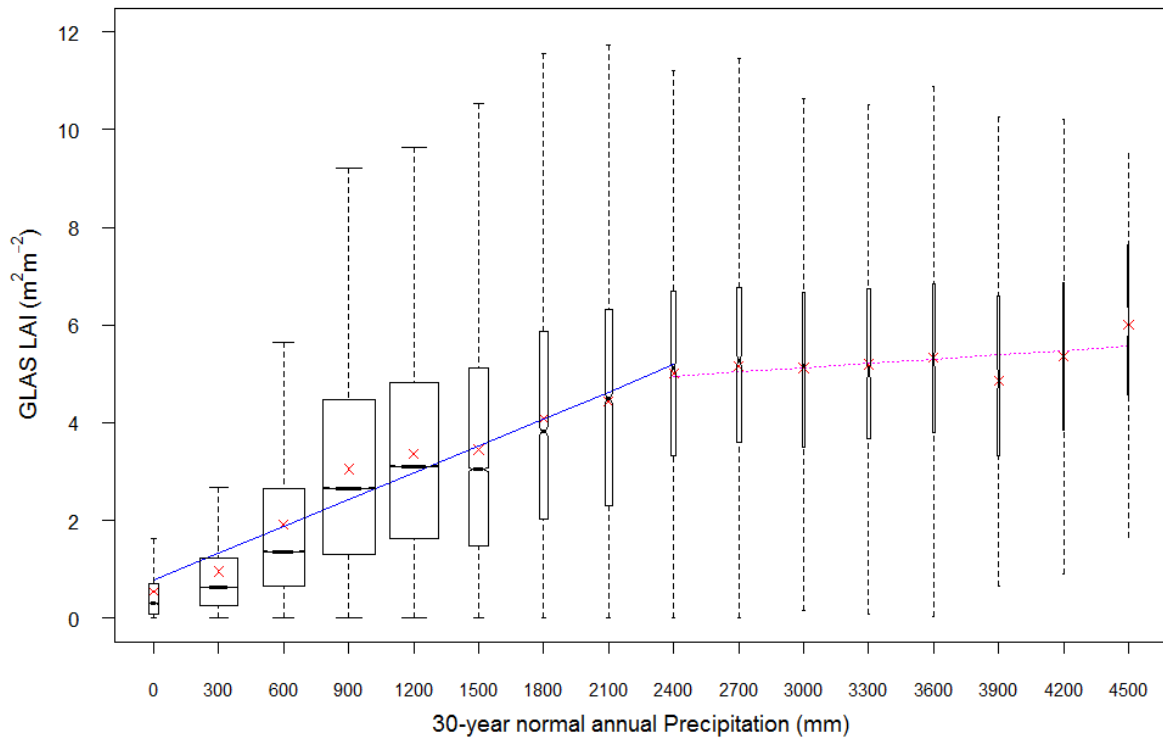


1

2 Fig. 8 Averaged GLAS VFP for different land cover types across US: non-forest vegetation types
 3 (left) and forest types (right). Mean values are central lines within the color-filled 95% CI
 4 envelope.



1
 2 Fig. 9 Distribution of GLAS LAI (left axis) and Forest Ratio - GLAS shots over forest divided by
 3 total shot numbers - (right axis). Overall, there is a decreasing trend of LAI values as elevation
 4 increases, but deviations occur from this trend that are associated with elevational variation in
 5 Forest Ratio, which was defined as the percentage of footprints classified as forests in total GLAS
 6 shots within each elevation group..
 7



1
 2 Fig. 10 Distribution of GLAS LAI as a function of precipitation. A linear regression analysis of
 3 LAI values averaged by precipitation groups shows an increasing trend up to areas of about 2400
 4 mm (blue line). Beyond this value the rate of change slows considerably (magenta line) but the
 5 trend is only weakly significant (P = 0.09).

6
 7